Concentration asymmetry and carbon enrichment in titanium carbide and silicon carbide clusters

José I. Martínez *
ESISNA Group, Institute of Materials Science of Madrid (ICMM-CSIC), University Campus of Cantoblanco, ES-28049 Madrid, Spain

Julio A. Alonso
Departamento de Física Teórica, Atómica y Optica, University of Valladolid, ES-47011 Valladolid, Spain

(Received 22 February 2022; accepted 9 May 2022; published 24 June 2022)

The mass spectra of metal clusters obtained by gas aggregation and laser vaporization techniques show variations of the abundance with cluster size, and the best-known manifestation is the magic numbers. The case of nanoalloys adds structural and chemical richness, and asymmetry in the atomic concentrations is sometimes observed. This is the case with Ti_xC_y and Si_xC_y clusters, for which the experiments performed until now reveal an enrichment of the clusters in carbon. The structure of the mass spectrum arises when hot clusters evaporate atoms to cool down. By performing density functional calculations, complemented by a thermochemical formalism to obtain Gibbs free energies, we have found that for each cluster in the families Ti_xC_y and Si_xC_y with $x = 1$–4 and $y = 1$–4, it is easier to remove titanium or silicon atoms as compared to removing carbon atoms, and this explains the carbon enrichment systematically observed in the experiments. The conclusion is that the broad compositional trends expected in the formation of alloy nanoclusters can be anticipated from calculations of the evaporation energies of the alloy components, and this may be particularly interesting in the field of catalysis.

DOI: 10.1103/PhysRevA.105.062820

I. INTRODUCTION

The properties of atomic clusters depend sensitively on the cluster size, in such a way that addition or extraction of just a single atom may change some properties of the cluster [1]. This sensitivity can be due to electronic effects, structural effects, or both. For instance, alkali-metal clusters show magic sizes for a number of atoms, $N = 2, 8, 20, 40, 58, 92,\ldots$, characterized by closed electronic shells. At those sizes, the stability drops drastically between sizes N and $N+1$, and this becomes reflected in a drop of the cluster size abundance in the mass spectrum [1–3]. A similar pronounced drop is observed in the ionization potential [1,3]. On the other hand, clusters formed by inert gas atoms or by some molecules display structural magic sizes, revealing onionlike icosahedral structures with an increasing number of closed atomic shells [1,4–6]. Another well-known case of pronounced structural stability is C_{60} [7]. Metallo-Carbohedrenes (met-cars), formed by carbon and transition-metal atoms, possess both structural and electronic stability [8–10]. Haruta and co-workers first noticed the size-dependent catalytic activity of small gold nanoparticles [11,12], which is a remarkable feature because bulk gold is a noble, unreactive metal. After that pioneering work, cluster and nanoparticle size has been confirmed to be a relevant parameter in the design of good catalysts [13–17].

When the clusters contain different atomic species, the relative concentration of the components affects the cluster properties, and this is an ingredient that can be used to tune the properties for specific applications [18]. In fact, the cluster structure is sensitive to the nature of the components and to their relative concentration. The parallel in the bulk case is the formation of solid metallic alloys, which adopt different structures depending on the temperature and the relative concentration of the component metals: solid solutions with the structure of the host for concentrations rich in one of the components, and intermetallic ordered compounds with specific stoichiometries and crystalline structures for one or several intermediate compositions (often, those stoichiometries are not too strict, allowing for a narrow range of compositions around the nominal one). The structure and the relative compositions of the intermediate compounds vary from alloy to alloy, manifesting in this way the richness of the alloy phase diagrams. In a similar way, nanoparticles and clusters formed by two or more types of atoms can display structural and chemical order, disorder, and segregation effects [18–21]. In addition, small clusters can form even in some cases in which the corresponding bulk solid alloys do not exist [22–27], which is an intrinsic size effect. Small alloy nanoclusters have a substantial fraction of atoms in their surface, and the preferred stoichiometries and the most stable structures vary as the cluster size increases. When binary alloy clusters form and grow in the usual gas aggregation methods, a larger variety of relative concentrations is detected in the mass spectra [28] as compared to the concentrations observed in the phase diagram of the bulk solid alloys. This is, again, an effect of the small size of the cluster, which enhances the mixing between the two components as compared to the bulk solid alloys. That is, a variety of stoichiometries A_xB_y can be expected, in general, in the mass spectra of small alloy nanoclusters. In addition, cluster growth can produce asymmetries in the concentration;

*joseignacio.martinez@icmm.csic.es

 ©2022 American Physical Society

for instance, concentrations rich in one of the components, or clusters with compositions around a specific one, A_xB_y [28].

Silicon carbide and titanium carbide clusters (Si_xC_y, Ti_xC_y) form two families where the concentration asymmetry, or enrichment in one component, i.e., carbon in this case, has been observed [8–10,28,29]. These clusters form part of the list of chemical substances that have been detected in the circumstellar atmospheres of low and intermediate mass stars in their late evolutionary stages [30]. Small clusters are the precursors of the interstellar dust, so knowing the trends in the relative concentrations in small Si_xC_y and Ti_xC_y clusters is important. By performing density functional calculations of the structure and Gibbs free energies of small carbide clusters as a function of size and relative concentration, we are able to identify and explain a tendency for carbon enrichment, which agrees with the phenomenology observed in the experimental mass spectra obtained by laser vaporization of solid samples in the Si_xC_y case [29], and by laser vaporization of Ti and reaction with a pulsed gas stream of small hydrocarbons in the Ti_xC_y case [28]. Herein, we propose that the key to explain the carbon enrichment consists in focusing on the evaporation energies, that is, the energies required to evaporate atoms when the clusters become hot as they grow.

II. THEORETICAL FRAMEWORK

A. Computational approach

Density functional theory (DFT) [31,32], as implemented in the GAUSSIAN16 atomistic simulation package [33], has been employed to investigate the electronic and atomic structures of small Si_xC_y and Ti_xC_y clusters. The Kohn-Sham monoelectronic wave functions and the electron densities have been calculated using an all-electron localized basis set formed with linear combinations of Gaussian functions: Dunning's correlation consistent triple zeta basis set (cc-pVTZ) [34]. Exchange and correlation effects between the electrons are treated by the Becke, three parameter, Lee-Yand Parr (B3LYP) hybrid functional [35–37], which includes 20% of exact exchange.

For each cluster size and composition, the ground-state structure has been calculated by starting with a large number of different atomic arrangements, taking information from the literature and adding many other candidates. All the inequivalent structural configurations (linear, planar, ringlike, three-dimensional polyhedra, etc.) and permutational isomers [38], that is, the same underlying structure but different distributions of the Ti (or Si) and C atoms over the available sites, and different spin multiplicities, have been investigated. All those structures were relaxed and fully optimized. A number of isomeric structures were then discovered (some of the starting atomic arrangements relax to the same isomer) and the structure with the lowest energy was identified as the ground-state structure. In this way, we are confident in obtaining, in each case, the lowest-energy structure and the structures of the low-lying isomers.

B. Thermochemical formalism

The thermal properties, as implemented in the GAUSSIAN package [39], will be used in the study of the evaporation of Si, Ti, and C atoms from the clusters. The Gibbs free energy G of a cluster at temperature T is defined as $G = H - TS$, where H is the enthalpy and S is the entropy. The enthalpy H is equal to the cluster total energy obtained from density functional theory, $E_{\rm DFT}$, corrected by the zero-point energy (ZPE) and by the internal thermal energy E_T. Thus, $G = E_{\rm DFT} + ZPE + E_T - TS$. The entropy and the thermal contribution to H are obtained from the partition function Z [40], which has electronic (e), translational (t), rotational (r), and vibrational (v) components [39]:

$$Z(N, V, T) = Z_e Z_t Z_r Z_v, \tag{1}$$

where N is the number of particles and V the volume.

After the partition function has been calculated, the molar values of the internal thermal energy E_T and the entropy S can be derived as follows:

$$E_T = \frac{RT^2}{Z}\left.\frac{\partial Z}{\partial V}\right|_V, \tag{2}$$

$$S = R\ln Z + \left.\frac{RT}{Z}\frac{\partial Z}{\partial V}\right|_V, \tag{3}$$

where R is the ideal gas constant. Here, we are only interested in values for not too low temperatures, $T \geqslant 50$ K. Accordingly, we write

$$Z_e = m, \tag{4}$$

$$Z_t = \left(\frac{2\pi M k_B T}{h^2}\right)^{\frac{3}{2}}\left(\frac{k_B T}{P}\right), \tag{5}$$

$$Z_r = \frac{1}{\sigma}\frac{T}{\Theta}\ \text{(for linear clusters)}, \tag{6}$$

$$= \sqrt{\frac{\pi}{\sigma^2}\frac{T^3}{\Theta}}\ \text{(for nonlinear clusters)}, \tag{7}$$

$$Z_v = \Pi_i\left[\frac{\exp\left(-\frac{\hbar\omega_i}{2k_BT}\right)}{1-\exp\left(-\frac{\hbar\omega_i}{k_BT}\right)}\right], \tag{8}$$

where h is the Planck constant ($\hbar = \frac{h}{2\pi}$), M the total mass, k_B the Boltzmann constant, m the spin multiplicity of the electronic state, and ω_i the vibrational frequency of the mode i [the product in Eq. (8) is taken over all vibrational modes with positive frequencies]. For linear clusters, $\Theta = \frac{h^2}{8\pi^2 k_B I}$ (I is the moment of inertia) and $\sigma = 1$ or 2, depending on whether the cluster is heteronuclear or homonuclear. For nonlinear clusters, $\Theta = \Theta_x\Theta_y\Theta_z$ (x, y, and z are the principal axes of the moment of inertia tensor) and σ is the order of the rotational subgroup in the point group associated to the cluster (see Table I). The thermochemical properties of the Si_xC_y and Ti_xC_y clusters have been computed at $T = 298.15$ K and P=1 bar.

III. STRUCTURE AND STABILITY OF THE CLUSTERS

A. Cluster structures

The calculated lowest-energy structures of Ti_xC_y and Si_xC_y clusters with $x = 1$–4 and $y = 1$–4 are reported in Fig. 1. We first focus on Si_xC_y. The clusters with a single Si atom are

TABLE I. Order of the rotational subgroup, σ, and spin multiplicity m, for the ground state of the Si_xC_y and Ti_xC_y clusters (with $x, y = 1$–4).

Si_xC_y	σ	m	Ti_xC_y	σ	m
SiC	1	3	TiC	1	3
SiC_2	2	1	TiC_2	1	3
SiC_3	1	3	TiC_3	2	1
SiC_4	1	1	TiC_4	2	3
Si_2C	2	1	Ti_2C	2	3
Si_2C_2	4	3	Ti_2C_2	4	1
Si_2C_3	1	1	Ti_2C_3	1	1
Si_2C_4	1	1	Ti_2C_4	1	1
Si_3C	2	1	Ti_3C	1	1
Si_3C_2	2	1	Ti_3C_2	2	1
Si_3C_3	2	1	Ti_3C_3	1	1
Si_3C_4	2	1	Ti_3C_4	2	1
Si_4C	1	1	Ti_4C	1	1
Si_4C_2	2	1	Ti_4C_2	2	1
Si_4C_3	1	1	Ti_4C_3	1	1
Si_4C_4	2	1	Ti_4C_4	12	1

linear, and the Si atom is located at one end of the chain. However, SiC_2, with the structure of an isosceles triangle, is an exception. Si_2C_3 and Si_2C_4 are again linear, with the Si atoms at the two ends of the chain. To some extent, this is also the case of Si_2C, which is an isosceles triangle with a large Si–C–Si angle of 123.6°. The structure of Si_2C_2, which is a rhombus, arises from that of SiC_2 by attaching a Si atom in a symmetric position to the first Si atom; but this structure can also be interpreted by starting with Si_2C and attaching a C atom in a symmetric position to the first C atom. The rest of the clusters are two dimensional, except the three-dimensional Si_4C and Si_4C_2. A noticeable feature is that in clusters with two or more C atoms, the C atoms form bonds with one or more C neighbors. In contrast, in clusters with two or more Si atoms, one can observe cases in which some Si atoms do not have Si neighbors. These results can be compared with previous work. The calculated structures of Si_3C (rhomboidal), Si_2C_3 (linear), Si_2C_2 (rhombic), and Si_3C_2 (irregular pentagon) are confirmed by vibrational spectroscopy and *ab initio* calculations [41–45]. The structures of SiC_2 and Si_2C are supported by spectroscopy [46–48] and by other experiments [49]. Si_4C is an interesting case. Its vibrational spectrum, measured by Truong *et al.* [45] was interpreted as revealing the presence of two isomers in the experiment. The lowest-energy isomer can be seen as two deformed trigonal pyramids sharing the base, and the other isomer corresponds to the structure shown in Fig. 1. The DFT-B3LYP calculations performed by Truong *et al.* [45] predict very similar total energies for these two isomers, with a difference of only 0.011 eV. Interestingly, other DFT studies [50–52], including our present work, and calculations by Truong *et al.* [45] using other quantum chemical methods, predict the inverse ordering between the two isomers, which is understandable because the two isomers are nearly degenerate in energy.

The structures of Ti_xC_y have been discussed in previous works [30,53], and only a comparison with the Si_xC_y structures is made here. Formation of linear chains in carbon-rich clusters is observed in Si_xC_y, but not in Ti_xC_y. A tendency to form compact three-dimensional structures is observed in Ti_xC_y, but not in Si_xC_y. This is because Ti is a transition-metal element, which tends to maximize the number of neighbors, whereas C and Si are elements in the same column of the Periodic Table, which tend to form covalent bonds with a small number of neighbors. A third difference is that C atoms not bonded to other C atoms exist in some Ti_xC_y clusters, but not in Si_xC_y.

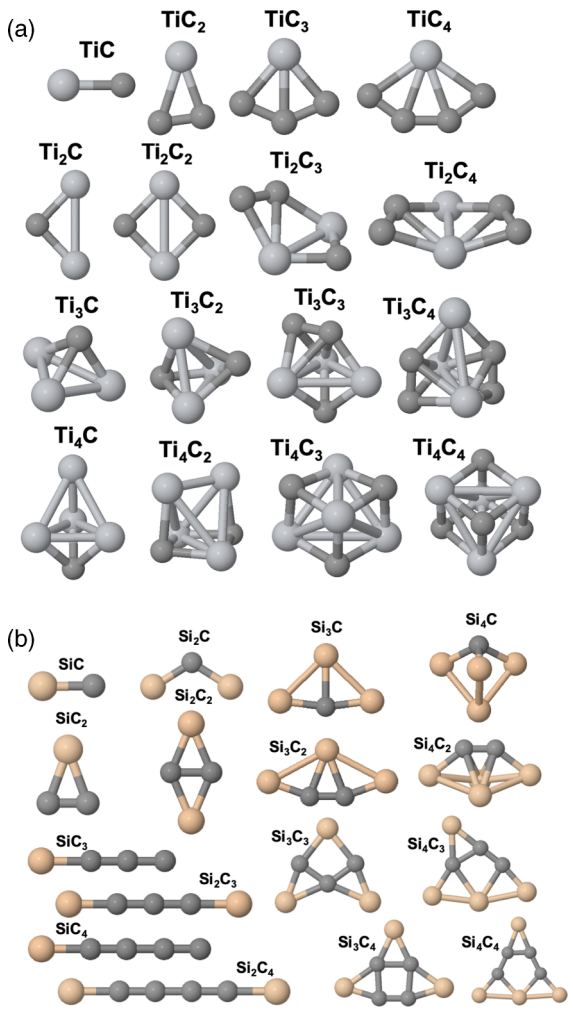

FIG. 1. Lowest-energy structures of (a) Ti_xC_y and (b) Si_xC_y clusters, with $x = 1$–4 and $y = 1$–4. Light gray, orange, and dark gray spheres represent Ti, Si, and C atoms, respectively.

B. Review of experimental phenomenology

Mass spectrometric studies of Ti-C clusters have been performed by several authors with a clear focus on the Ti_8C_{12} metallo-carbohedrene [8–10,28]. The clusters were formed by laser vaporization of Ti and reaction with a pulsed gas stream of small hydrocarbons. Apart from the prominent abundance of Ti_8C_{12} in the mass spectra, those works also give valuable information on other cluster sizes and compositions. The most striking observation is the asymmetry

TABLE II. Evaporation energies of carbon and titanium atoms, $E_{\text{evap C}}$ and $E_{\text{evap Ti}}$, from Ti_xC_y clusters, and the difference between them, $\Delta E_{\text{evap C-Ti}} = E_{\text{evap C}} - E_{\text{evap Ti}}$. Also, evaporation Gibbs free energies, $G_{\text{evap C}}$ and $G_{\text{evap Ti}}$ at 298.15 K and 1 atm, and their difference.

$E_{\text{evap C}}$					$G_{\text{evap C}}$				
x/y	1	2	3	4	x/y	1	2	3	4
1	3.61	8.35	6.12	7.18	1	3.74	8.43	6.37	7.18
2	6.25	6.49	7.02	7.15	2	6.19	6.97	6.93	7.39
3	7.26	8.27	7.41	7.36	3	7.68	8.55	7.38	7.13
4	8.49	8.79	8.13	9.15	4	9.20	8.53	8.03	8.92
$E_{\text{evap Ti}}$					$G_{\text{evap Ti}}$				
x/y	1	2	3	4	x/y	1	2	3	4
1	3.61	5.95	4.40	6.95	1	3.74	6.54	5.67	5.54
2	3.59	1.73	2.63	2.60	2	3.09	1.63	2.19	2.40
3	1.05	2.83	3.23	3.44	3	1.15	2.74	3.19	2.93
4	2.08	2.61	3.33	5.11	4	2.09	2.07	2.72	4.51
$\Delta E_{\text{evap C-Ti}}$					$\Delta G_{\text{evap C-Ti}}$				
x/y	1	2	3	4	x/y	1	2	3	4
1	0.00	2.40	1.72	0.22	1	0.00	1.89	0.70	1.65
2	2.66	4.76	4.39	4.55	2	3.09	5.34	4.74	5.00
3	6.21	5.44	4.18	3.92	3	6.52	5.81	4.19	4.20
4	6.41	6.19	4.80	4.03	4	7.11	6.46	5.31	4.41

in the composition of the clusters: in general, the detected clusters are rich in carbon. The abundances are most prominent at the compositions Ti_xC_{2x} or Ti_xC_{2x-1}, but in each family with a specific number x of Ti atoms, an envelope of clusters with compositions Ti_xC_{2x-2}, Ti_xC_{2x-1}, Ti_xC_{2x}, Ti_xC_{2x+1}, Ti_xC_{2x+2} and substantial abundances are detected. The family Ti_8C_y represents an interesting exception: the high abundance envelope is centered on Ti_8C_{12}, the met-car, whose atomic and electronic structures have been discussed at length [54–56], although the enrichment in carbon is also evident. Experiments of laser photodissociation of size-selected Ti_xC_y clusters reveal the loss of Ti atoms [57,58], confirming the enrichment in carbon. Of course, the observed carbon enrichment is restricted to small clusters because the solid-state Ti-C phase diagram [59] shows a single compound centered at the composition $Ti_{55}C_{45}$. Then, a shift towards near equiatomic compositions is expected for medium- or large-size clusters, and this shift has been observed by Pilgrim and Duncan [57], who interpreted those clusters as nanofragments of a face-centered-cubic (fcc) crystal lattice.

Si_xC_y clusters in a wide range of sizes (up to about 100 atoms) were produced by Pellarin *et al.* [29] in a laser vaporization source. The targets were stoichiometric SiC crystalline rods and composite rods of different compositions formed from graphite and silicon powders. The analysis of the mass spectra and of the products of photodissociation of mass-selected clusters revealed enrichment in carbon. This enrichment also occurs in the sublimation of bulk silicon carbide, in which case the dominant process is the evaporation of silicon atoms [49].

In the experiments producing Ti_xC_y clusters, a high-power laser evaporates Ti atoms from a metal rod, and the sticking of the atoms in the metal vapor leads to the formation and growth of Ti clusters. A gas stream formed by small hydrocarbon molecules (CH_4, C_2H_4, or others) serves as a heat bath to cool the metal vapor, and at the same time is the reactant gas. Fast dehydrogenation reactions between the hydrocarbons and the Ti clusters lead to the formation of Ti_xC_y clusters. The processes in the formation of Si_xC_y clusters are a bit different. The irradiated targets were Si-C solid composites and the cooling gas was He.

The formation and growth of clusters obtained by gas aggregation techniques, in particular those of interest in this work, are controlled by the adsorption cross section of monomer units (atoms, in general, but molecules in the case of molecular clusters), which is the product of a geometrical cross section slowly varying with cluster size, and a sticking coefficient usually close to one [60]. The addition of dimers and agglomeration of larger clusters is less probable and only occurs at a later stage, when the highly mobile monomers have been exhausted, or under higher pressures. At this stage, the population distribution in terms of cluster size will be rather featureless and magic-size clusters are not expected to be prominent. On the other hand, the mean composition of the clusters will reflect the stoichiometry of the laser-induced plasma, especially for Si_xC_y cluster formation, in which case the plasma is directly generated from Si-C solid composite targets of specific compositions [29]. A smooth and featureless mass spectrum would then be observed if the collisional cooling of the clusters by the gas heat bath between subsequent growth steps is efficient enough. However, in practice, the cooling of the clusters is not complete. The heat of condensation is not fully transferred to the heat bath, and the Ti_xC_y and Si_xC_y clusters warm up and become vibrationally hot as they grow. Then, an important backwards effect takes place: when the cluster is warm enough, energy is released by evaporating mainly atoms and sometimes small fragments. This is the process giving rise to the structure in the abundance mass spectra of all kinds of clusters produced by these methods [1]. In particular, this

TABLE III. Evaporation energies of carbon and silicon atoms, $E_{\text{evap C}}$ and $E_{\text{evap Si}}$, from Si_xC_y clusters, and the difference between them, $\Delta E_{\text{evap C-Si}} = E_{\text{evap C}} - E_{\text{evap Si}}$. Also, evaporation Gibbs free energies, $G_{\text{evap C}}$ and $G_{\text{evap Si}}$ at 298.15 K and 1 atm, and their difference.

$E_{\text{evap C}}$					$G_{\text{evap C}}$				
x/y	1	2	3	4	x/y	1	2	3	4
1	4.29	8.35	5.42	7.28	1	4.82	8.33	5.29	7.14
2	4.81	8.54	7.06	5.37	2	4.84	8.40	6.93	5.30
3	7.48	6.01	4.63	6.45	3	7.39	5.92	4.57	6.32
4	7.04	6.82	5.36	6.31	4	6.93	6.68	5.30	6.21
$E_{\text{evap Si}}$					$G_{\text{evap Si}}$				
x/y	1	2	3	4	x/y	1	2	3	4
1	4.29	6.46	4.18	6.00	1	4.82	6.55	4.57	6.26
2	3.73	3.92	5.57	3.67	2	3.82	3.88	5.53	3.68
3	6.42	3.88	1.44	2.53	3	6.39	3.91	1.55	2.57
4	3.00	3.82	4.55	4.41	4	3.02	3.78	4.51	4.40
$\Delta E_{\text{evap C-Si}}$					$\Delta G_{\text{evap C-Si}}$				
x/y	1	2	3	4	x/y	1	2	3	4
1	0.00	1.88	1.24	1.27	1	0.00	1.78	0.72	0.89
2	1.08	4.61	1.49	1.70	2	1.02	4.51	1.41	1.62
3	1.06	2.12	3.18	3.92	3	1.00	2.01	3.02	3.75
4	4.04	3.00	0.81	1.90	4	3.91	2.90	0.79	1.81

is the way the magic numbers appear in the mass spectrum because the population of magic clusters, being these are especially stable and less prone to evaporate, is enriched in the cluster beam by the evaporation events of larger clusters [1–5,7,8]. It then becomes clear that the physical quantity that has to be investigated to understand the features of the mass spectra is the evaporation energy of atoms from the clusters.

C. Atom evaporation and carbon enrichment

The dissociation processes of interest are those in which a Ti or a C atom is evaporated from Ti_xC_y, and a Si or a C atom is evaporated from Si_xC_y:

$$Ti_xC_y \rightarrow Ti_{x-1}C_y + Ti, \tag{9}$$

$$Ti_xC_y \rightarrow Ti_xC_{y-1} + C, \tag{10}$$

$$Si_xC_y \rightarrow Si_{x-1}C_y + Si, \tag{11}$$

$$Si_xC_y \rightarrow Si_xC_{y-1} + C. \tag{12}$$

The energies required to evaporate a C or a Ti atom from the clusters are given, in terms of DFT energies of the products and the initial cluster, by

$$E_{\text{evapTi}}[Ti_xC_y] = E[Ti_{x-1}C_y] + E[Ti] - E[Ti_xC_y], \tag{13}$$

$$E_{\text{evapC}[Ti_xC_y]} = E[Ti_xC_{y-1}] + E[C] - E[Ti_xC_y], \tag{14}$$

$$E_{\text{evapSi}}[Si_xC_y] = E[Si_{x-1}C_y] + E[Si] - E[Si_xC_y], \tag{15}$$

$$E_{\text{evapC}}[Si_xC_y] = E[Si_xC_{y-1}] + E[C] - E[Si_xC_y], \tag{16}$$

and the corresponding Gibbs free energies at $T = 298.15$ K and P=1 bar,

$$G_{\text{evapTi}}[Ti_xC_y] = G[Ti_{x-1}C_y] + G[Ti] - G[Ti_xC_y], \tag{17}$$

$$G_{\text{evapC}}[Ti_xC_y] = G[Ti_xC_{y-1}] + G[C] - G[Ti_xC_y], \tag{18}$$

$$G_{\text{evapSi}}[Si_xC_y] = G[Si_{x-1}C_y] + G[Si] - G[Si_xC_y], \tag{19}$$

$$G_{\text{evapC}}[Si_xC_y] = G[Si_xC_{y-1}] + G[C] - G[Si_xC_y]. \tag{20}$$

The DFT evaporation energies and the evaporation Gibbs free energies of Ti_xC_y and Si_xC_y clusters are given in Table II and Table III, respectively. All the evaporation energies have positive values because the process is endothermic. The trends are better appreciated in Figs. 2 and 3, where the results for the evaporation free energies are presented in the form of histograms, in which clusters with the same initial number of Ti (or Si) atoms are represented by the same color. A second observation is that in all clusters, the energies (and free energies) required to evaporate C atoms are higher than those to evaporate Ti or Si atoms. This is clear in Fig. 4, where the

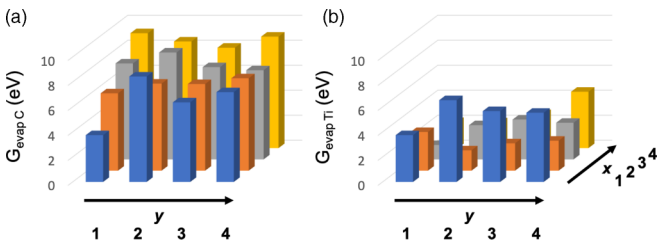

FIG. 2. Histograms showing the Gibbs free energies (in eV) for the evaporation of (a) a C atom, $G_{\text{evap C}}$, and (b) a Ti atom, $G_{\text{evap Ti}}$, in Ti_xC_y clusters with x = 1–4 and y = 1–4. Clusters with the same number x of Ti atoms are represented by bars of the same color.

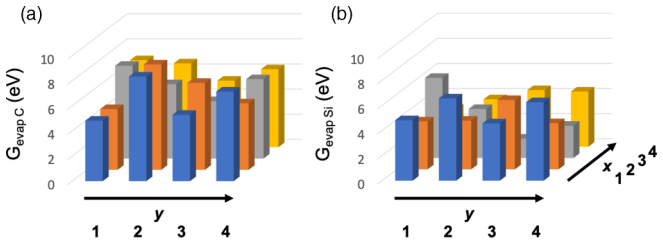

FIG. 3. Histograms showing the Gibbs free energies (in eV) for the evaporation of (a) a C atom, $G_{evap\ C}$, and (b) a Si atom, $G_{evap\ Si}$, in Si_xC_y clusters with $x = 1$–4 and $y = 1$–4. Clusters with the same number x of Si atoms are represented by bars of the same color.

differences between the evaporation free energies of C and Ti (or Si) atoms are plotted for Ti_xC_y (and Si_xC_y) clusters,

$$\Delta G_{evap\ C\text{-}Ti}[Ti_xC_y] = G_{evap\ C}[Ti_xC_y] - G_{evap\ Ti}[Ti_xC_y], \quad (21)$$

$$\Delta G_{evap\ C\text{-}Si}[Si_xC_y] = G_{evap\ C}[Si_xC_y] - G_{evap\ Si}[Si_xC_y]. \quad (22)$$

The differences between the DFT evaporation energies, $\Delta E_{evap\ C\text{-}Ti} = E_{evap\ C} - E_{evap\ Ti}$ and $\Delta E_{evap\ C\text{-}Si} = E_{evap\ C} - E_{evap\ Si}$, are also plotted in Fig. 4, and one can observe that DFT energies and Gibbs free energies deliver very similar quantitative results. In all cases, evaporating C atoms is substantially more difficult than evaporating Ti or Si atoms from the clusters. And the differences between the DFT evaporation energies, or between the evaporation free energies, are larger in Ti_xC_y as compared to Si_xC_y clusters. The evaporation free energies have been calculated for specific conditions, $T = 298.15$ K and P=1 bar, which do not necessarily coincide with the conditions applying to the experiments of cluster formation, where the pressures in the vacuum chamber can be much lower [28]. But the similarity of the qualitative picture (and the quantitative results) obtained with DFT evaporation energies, on one hand, and with evaporation free energies, on the other hand, displayed in Tables II and III and in Figs. 2–4, indicate that thermal and pressure effects are not critical in the calculations.

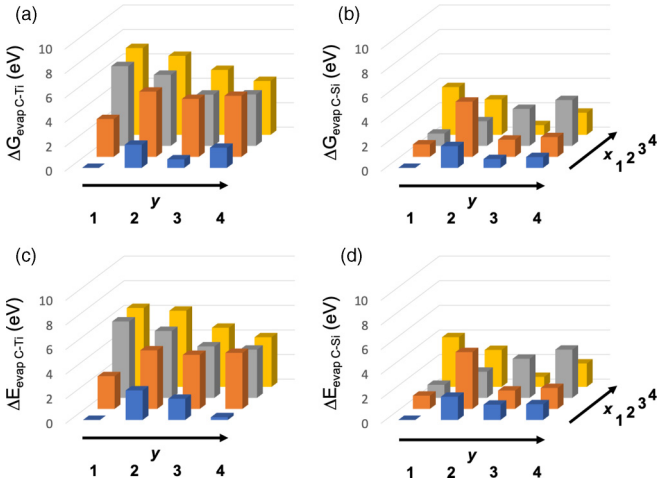

FIG. 4. Histograms showing (a) the Gibbs free-energy difference, $\Delta G_{evap\ C\text{-}Ti}$, between the evaporation of a Ti atom and a C atom from Ti_xC_y, and (b) the Gibbs free-energy difference, $\Delta G_{evap\ C\text{-}Si}$, between the evaporation of a Si atom and a C atom from Si_xC_y. Clusters with the same number x of Ti (or Si) atoms are represented by bars of the same color. All results are in eV. (c) and (d) provide similar information for DFT evaporation energy differences, $\Delta E_{evap\ C\text{-}Ti}$ and $\Delta E_{evap\ C\text{-}Si}$.

As discussed above, when clusters form in a gas aggregation experiment, the structure of the abundance spectrum detected by mass spectrometry arises as a result of a two-step process. In the first step, clusters grow mainly by the successive addition of atoms of the species present in the vapor [1], and this gives rise to a smooth population distribution. But the process of condensation is exothermic and the clusters become hot (especially vibrationally) as they grow. A good part of the internal heat can be released by collisional cooling with a carrier gas. However, another part still remains stored in the clusters and when these are warm enough, energy is released by evaporating atoms. This evaporative cooling mechanism gives structure to the mass spectrum. In the case of Ti_xC_y and Si_xC_y clusters, the evaporation free energies of C and Ti (or Si) atoms are quite different. Evaporation of Ti or Si atoms is easier than evaporation of C atoms, and the clusters will be enriched in carbon. This enrichment is precisely what the experiments reveal. Figure 4 shows that the effect is more pronounced in the Ti_xC_y clusters; that is, the values of $\Delta E_{evap\ C\text{-}Ti}$ are, in most cases, larger than the values of $\Delta E_{evap\ C\text{-}Si}$. A discernible trend is that with few exceptions, $\Delta E_{evap\ C\text{-}Ti}$ increases as the number of Ti atoms in the initial cluster increases. We see clear examples in the series TiC, Ti_2C, Ti_3C, Ti_4C, and in the series TiC_2, Ti_2C_2, Ti_3C_2, Ti_4C_2. A similar trend can be roughly observed in $\Delta E_{evap\ C\text{-}Si}$, but with more exceptions. An alternative way of viewing this trend is that the tendency for carbon enrichment by Ti or Si evaporation is more pronounced when the original cluster composition is poor in C.

The results in Fig. 4 appear to be quite robust, since no exception is found to the rule that the evaporation of C from the Ti_xC_y and Si_xC_y clusters is more costly than the evaporation of Ti or Si. For this reason, one can confidently expect that the rule will also be valid in a wider range of sizes. In fact, other experimental observations of carbon enrichment can be explained by the larger carbon evaporation energies. One of these is the observation of prompt and delayed Ti^+ emission after multiphoton excitation of the Ti_8C_{12} met-car [58]. The delayed emission is interpreted as the excitation of a collective giant dipole resonance that later decays by emission of Ti^+ [55,56]. In both cases, i.e., prompt and delayed processes, the emission of Ti^+ (and not C^+) is explained by the lower evaporation energy of Ti. But it is clear that the C enrichment shown by these experiments, and in general the concentration asymmetry observed in the mass spectrometry experiments, has to change to a situation of concentration symmetry (Ti_xC_x and Si_xC_x) as the cluster size becomes sufficiently large because the bulk alloys have near-equiatomic stoichiometries, TiC and SiC [59,61].

IV. CONCLUSIONS

Knowledge of the atomic concentrations most likely to be obtained in binary or multicomponent alloy clusters

and nanoparticles formed by gas aggregation and laser vaporization techniques is technologically important for the applications of those clusters and nanoparticles in catalysis and other fields. Taking small Ti_xC_y and Si_xC_y clusters as a case study, previous experimental work has revealed an asymmetry in the atomic concentration: the clusters detected by mass spectrometry are rich in carbon. By performing DFT calculations, we have found that the evaporation energies of the different types of atoms forming the nanoalloy (Ti versus C, or Si versus C) are the key ingredients to explain the asymmetry of the concentration and the enrichment of these nanoalloys in carbon. For each one of the 16 clusters in the Ti_xC_y and Si_xC_y families with $x = 1$–4 and $y = 1$–4, the energy required to remove a carbon atom from the cluster is always higher than the energy to remove a Ti (or a Si) atom. Since the structure of the mass spectra arises when hot clusters evaporate atoms to cool down, this asymmetry in the evaporation energy leads to the observed carbon enrichment. This rule, which we expect to be valid for other nanoalloys, will allow one to anticipate broad trends in their compositions.

ACKNOWLEDGMENTS

This work was supported by the Ministerio de Ciencia e Innovación of Spain (Grants No. PID2020-113142RB-C21, No. PLEC2021-007906, and No. PID2019-104924RB-I00, funded MCIN/AEI/10.13039/501100011033), Comunidad de Madrid (Grants No. S2018/NMT-4367 and No. Y2020/NMT-6469), and University of Valladolid (GIR Nanostructure Physics).

[1] J. A. Alonso, *Structure and Properties of Atomic Nanoclusters* (Imperial College Press, London, 2011).

[2] W. D. Knight, K. Clemenger, W. A. de Heer, W. A. Saunders, M. Y. Chou, and M. L. Cohen, Electronic Shell Structure and Abundances of Sodium Clusters, Phys. Rev. Lett. **52**, 2141 (1984).

[3] W. A. de Heer, The physics of simple metal clusters: Experimental aspects and simple models, Rev. Mod. Phys. **65**, 611 (1993).

[4] O. Echt, K. Sattler, and E. Recknagel, Magic Numbers for Sphere Packings: Experimental Verification in Free Xenon Clusters, Phys. Rev. Lett. **47**, 1121 (1981).

[5] O. Echt, O. Kandler, T. Leisner, W. Miehle, and E. Recknagel, Magic numbers in mass spectra of large van der Waals clusters, J. Chem. Soc. Faraday Trans. **86**, 2411 (1990).

[6] J. I. Martínez, M. Isla, and J. A. Alonso, Theoretical study of molecular hydrogen clusters, Eur. Phys. J. D **43**, 61 (2007).

[7] H. W. Kroto, J. R. Heath, S. C. O'Brien, R. F. Curl, and R. E. Smalley, C60: Buckminsterfullerene, Nature (London) **318**, 162 (1985).

[8] B. C. Guo, K. P. Kerns, and A. W. Castleman, $Ti_8C_{12}^+$ Metallo-Carbohedrenes: A new class of molecular clusters? Science **255**, 1411 (1992).

[9] B. C. Guo, S. Wei, J. Purnell, S. Buzza, and A. W. Castleman, Metallo-carbohedrenes $M_8C_{12}^+$ (M = V, Zr, Hf and Ti): A class of stable molecular cluster ions, Science **256**, 515 (1992).

[10] S. Wei Jr., B. C. Guo, J. Purnell, S. Buzza, and A. W. Castleman, Metallo-Carbohedrenes as a class of stable neutral clusters: Formation mechanism of $M_8C_{12}^+$ (M = Ti and V), J. Phys. Chem. **96**, 4166 (1992).

[11] T. Hayashi, K. Tanaka, and M. M. Haruta, Selective vapor-phase epoxidation of propylene over Au/TiO_2 catalysts in the presence of oxygen and hydrogen, J. Catal. **178**, 566 (1998).

[12] M. Haruta, N. Yamada, T. Kobayashi, and S. Iijima, Gold catalysts prepared by coprecipitation for low-temperature oxidation of hydrogen and of carbon monoxide, J. Catal. **115**, 301 (1989).

[13] B. Zandkarimi and A. N. Alexandrova, Dynamics of sub-nanometer Pt clusters can break the scaling relationships in catalysis, J. Phys. Chem. Lett. **10**, 460 (2019).

[14] A. Halder, L. A. Curtiss, A. Fortunelli, and S. Vajda, Perspective: Size selected clusters for catalysis and electrochemistry, J. Chem. Phys. **148**, 110901 (2018).

[15] S. M. Lang, I. Fleischer, T. M. Bernhardt, R. N. Barnett, and U. Landman, Low-temperature CO oxidation catalyzed by free palladium clusters: Similarities and differences to Pd surfaces and supported particles, ACS Catal. **5**, 2275 (2015).

[16] Y. Lei, F. Mehmood, S. Lee, J. Greeley, B. Lee, S. Seifert, R. E. Winans, J. W. Elam, R. J. Meyer, P. C. Redfern, D. Teschner, R. Schlögl, M. J. Pellin, L. A. Curtiss, and S. Vajda, Increased silver activity for direct propylene epoxidation via subnanometer size effects, Science **328**, 224 (2010).

[17] L. M. Molina, S. Lee, K. Sell, G. Barcaro, A. Fortunelli, B. Lee, S. Seifert, R. E. Winans, J. W. Elam, M. J. Pellin, I. Barke, V. von Oeynhausen, Y. Lei, R. J. Meyer, J. A. Alonso, A. Fraile Rodríguez, A. Kleibert, S. Giorgio, C. R. Henry, K.-H. Meiwes-Broer, and S. Vajda, Size-dependent selectivity and activity of silver nanoclusters in the partial oxidation of propylene to propylene oxide and acrolein: A joint experimental and theoretical study, Catal. Today **160**, 116 (2011).

[18] R. Ferrando, J. Jellinek, and R. L. Johnston, Nanoalloys: From theory to applications of alloy clusters and nanoparticles, Chem. Rev. **108**, 845 (2008).

[19] J. M. Montejano-Carrizales, M. P. Iñiguez, and J. A. Alonso, Embedded-atom method applied to bimetallic clusters: The Cu-Ni and Cu-Pd systems, Phys. Rev. B **49**, 16649 (1994).

[20] R. Ferrando, Determining the equilibrium structures of nanoalloys by computational methods, J. Nanopart. Res. **20**, 179 (2018).

[21] J.-Q. Goh, J. Akola, and R. Ferrando, Geometric structure and chemical ordering of large Au-Cu clusters: A computational study, J. Phys. Chem. C **121**, 10809 (2017).

[22] S. Neukermans, E. Janssens, Z. F. Chen, R. E. Silverans, P. v. R. Schleyer, and P. Lievens, Extremely Stable Metal-Encapsulated $AlPb_{10}^+$ and $AlPb_{12}^+$ Clusters: Mass-Spectrometric Discovery and Density Functional Theory Study, Phys. Rev. Lett. **92**, 163401 (2004).

[23] Z. Chen, S. Neukermans, X. Wang, E. Janssens, Z. Zhou, R. E. Silverans, R. B. King, P. v. R. Schleyer, and P. Lievens, To achieve stable spherical clusters: General principles and experimental confirmations, J. Am. Chem. Soc. **128**, 12829 (2006).

[24] S. Bhattacharyya, T. T. Nguyen, J. De Haeck, K. Hansen, P. Lievens, and E. Janssens, Mass-selected photodissociation studies of $AlPb_n^+$ clusters (n=7–16): Evidence for the extraordinary stability of $AlPb_{10}^+$ and $AlPb_{12}^+$, Phys. Rev. B **87**, 054103 (2013).

[25] A. Donís, M. J. López, and J. A. Alonso, Bimetallic Al–Sn clusters: Mixing at the nanoscale, Phys. Chem. Chem. Phys. **21**, 22919 (2019).

[26] E. Janssens, T. Van Hoof, N. Veldeman, S. Neukermans, M. Hou, and P. Lievens, Mass spectrometric and modeling investigations of bimetallic silver–cobalt clusters, Intl. J. Mass Spectrom. **252**, 38 (2006).

[27] P. Marín, J. A. Alonso, E. Germán, and M. J. López, Nanoalloys of metals which do not form bulk alloys: The case of Ag-Co, J. Phys. Chem. A **124**, 6468 (2020).

[28] H. Yu, M. G. Huber, and F. W. Froben, Laser ablation of refractory material, cluster formation and deposition, Appl. Surf. Sci. **86**, 74 (1995).

[29] M. Pellarin, C. Ray, P. Mélinon, J. Lermé, J. L. Vialle, P. Kéghélian, A. Perez, and M. Broyer, Silicon-carbon mixed clusters, Chem. Phys. Lett. **277**, 96 (1997).

[30] M. Agúndez, J. I. Martínez, P. L. de Andres, J. Cernicharo, and J. A. Martín-Gago, Chemical equilibrium in AGB atmospheres: Successes, failures, and prospects for small molecules, clusters, and condensates, Astron. Astrophys. **637**, A59 (2020).

[31] W. Kohn and L. J. Sham, Self-consistent equations including exchange and correlation effects, Phys. Rev. **140**, A1133 (1965).

[32] D. S. Sholl and J. A. Steckel, *Density Functional Theory* (Wiley, Hoboken, New Jersey, 2009).

[33] M. J. Frisch, G. W. Trucks, H. B. Schlegel, G. E. Scuseria, M. A. Robb, J. R. Cheeseman, G. Scalmani, V. Barone, G. A. Petersson, H. Nakatsuji, X. Li, M. Caricato, A. V. Marenich, J. Bloino, B. G. Janesko, R. Gomperts, B. Mennucci, H. P. Hratchian, J. V. Ortiz, A. F. Izmaylov *et al.*, Computer code Gaussian16, Rev. C.01 (Gaussian Inc. Wallingford, CT, 2016), https://gaussian.com.

[34] T. H. Dunning, Gaussian basis sets for use in correlated molecular calculations. I. The atoms boron through neon and hydrogen, J. Chem. Phys. **90**, 1007 (1989).

[35] C. Lee, W. Yang, and R. G. Parr, Development of the Colle-Salvetti correlation-energy formula into a functional of the electron density, Phys. Rev. B **37**, 785 (1988).

[36] A. D. Becke, A new mixing of Hartree-Fock and local density functional theories, J. Chem. Phys. **98**, 1372 (1993).

[37] A. D. Becke, Density functional thermochemistry. III. The role of exact exchange, J. Chem. Phys. **98**, 5648 (1993).

[38] M. J. López, P. A. Marcos, and J. A. Alonso, Structural and dynamical properties of Cu-Au bimetallic clusters, J. Chem. Phys. **104**, 1056 (1996).

[39] J. W. Ochterski, Thermochemistry in Gaussian (Gaussian Inc., Wallingford, CT, 2000), pp. 1–19.

[40] M. Kardar, *Statistical Physics of Particles* (Cambridge University Press, Cambridge, 2007).

[41] J. D. Presilla-Márquez and W. R. M. Graham, Vibrational spectra of tetra-atomic silicon-carbon clusters. I. Rhomboidal Si_3C in Ar at 10 K, J. Chem. Phys. **96**, 6509 (1992).

[42] J. D. Presilla-Márquez and W. R. M. Graham, Vibrational spectra of penta-atomic silicon-carbon clusters. II. Linear Si_2C_3, J. Chem. Phys. **100**, 181 (1994).

[43] J. D. Presilla-Márquez, S. C. Gay, C. M. L. Rittby, and W. R. M. Graham, Vibrational spectra of tetra-atomic silicon-carbon clusters. II. Si_2C_2 in Ar at 10 K, J. Chem. Phys. **102**, 6354 (1995).

[44] J. D. Presilla-Márquez, C. M. L. Rittby, and W. R. M. Graham, Vibrational spectra of pentaatomic silicon-carbon clusters. III. Pentagonal Si_3C_2, J. Chem. Phys. **104**, 2818 (1996).

[45] N. X. Truong, M. Savoca, D. J. Harding, A. Fielicke, and O. Dopfer, Vibrational spectra and structures of Si_nC clusters (n = 3–8), Phys. Chem. Chem. Phys. **17**, 18961 (2015).

[46] H. Bredohl, I. Dubois, H. Leclercq, and F. Mélen, Rotational analysis of the 000-000 and 010-000 bands of SiC_2, J. Mol. Spectrosc. **128**, 399 (1988).

[47] Z. H. Kafafi, R. H. Hauge, L. Fredin, and J. L. Margrave, Infrared matrix isolation spectrum of the disilicon carbide (Si_2C) molecule, J. Phys. Chem. **87**, 797 (1983).

[48] J. D. Presilla-Márquez and W. R. M. Graham, Fourier transform vibrational spectroscopy of Si_2C in solid Ar, J. Chem. Phys. **95**, 5612 (1991).

[49] R. W. Schmude and K. A. Gingerich, Thermodynamic study of small silicon carbide clusters with a mass spectrometer, J. Phys. Chem. A **101**, 2610 (1997).

[50] A. Nakajima, T. Taguwa, K. Nakao, M. Gomei, R. Kishi, S. Iwata, and K. Kaya, Photoelectron spectroscopy of silicon-carbon cluster anions ($Si_nC_m^-$), J. Chem. Phys. **103**, 2050 (1995).

[51] R. Kishi, M. Gomei, A. Nakajima, S. Iwata, and K. Kaya, Theoretical study of carbon doped small silicon clusters: Electron affinities of Si_nC (n=2–5), J. Chem. Phys. **104**, 8593 (1996).

[52] B.-X. Chu, Q-Y. Li, and J. Yu, Stability of carbon-doped silicon clusters: (FP-LMTO) molecular dynamics calculations, J. Mol. Struct. (THEOCHEM) **806**, 67 (2007).

[53] S. Gámez-Valenzuela, J. A. Alonso, G. Santoro, and J. I. Martínez, Structure, stability, and optical absorption spectra of small Ti_nC_x clusters: A first-principles approach, MNRAS **508**, 5074 (2021).

[54] M.-M. Rohmer, M. Bénard, and J.-M. Poblet, Structure, reactivity, and growth pathways of metallocarbohedrenes M_8C_{12} and transition metal/carbon clusters and nanocrystals: A challenge to computational chemistry, Chem. Rev. **100**, 495 (2000).

[55] J. I. Martínez, A. Castro, A. Rubio, J. M. Poblet, and J. A. Alonso, Calculation of the optical spectrum of the Ti_8C_{12} and V_8C_{12} Met-cars, Chem. Phys. Lett. **398**, 292 (2004).

[56] J. I. Martínez, A. Castro, A. Rubio, and J. A. Alonso, Photoabsorption spectra of Ti_8C_{12} Metallo-Carbohedrynes: Theoretical spectroscopy within time-dependent density functional theory, J. Chem. Phys. **125**, 074311 (2006).

[57] J. S. Pilgrim and M. A. Duncan, Beyond Metallo-Carbohedrenes: growth and decomposition of metal-carbon nanocrystals, J. Am. Chem. Soc. **115**, 9724 (1993).

[58] B. D. May, S. F. Cartier, and A. W. Castleman, Delayed ionization and delayed atomic ion emission of Ti and V Metallo-Carbohedrenes. Evidence for collective electronic effects, Chem. Phys. Lett. **242**, 265 (1995).

[59] H. Okamoto, C-Ti (Carbon-Titanium), J. Phase Equilib. **19**, 89 (1998).

[60] J. M. Soler, N. García, O. Echt, K. Sattler, and E. Recknagel, Microcluster Growth: Transition from Successive Monomer Addition to Coagulation, Phys. Rev. Lett. **49**, 1857 (1982).

[61] S. Kawanishi, T. Yoshikawa, and T. Tanaka, Equilibrium phase relationship between SiC and a liquid phase in the Fe-Si-C system at 1523–1723 K, Mater. Trans. **50**, 806 (2009).